C. R. Geoscience 348 (2016) 598–608

Contents lists available at ScienceDirect

Comptes Rendus Geoscience

www.sciencedirect.com

Hydrology, Environment (Surface Geochemistry)

Investigation of the nature and origin of the geological matrices rich in selenium within the Hydrogeological Experimental Site of Poitiers, France

Joseph Bassil [a,b,*], Aude Naveau [a], Claude Fontaine [a], Laurent Grasset [a], Jacques Bodin [a], Gilles Porel [a], Moumtaz Razack [a], Véronique Kazpard [b], Speranta-Maria Popescu [c]

[a] CNRS, UMR 7285, Institut de chimie des milieux et matériaux de Poitiers (IC2MP), Université de Poitiers, bâtiment B8, rue Michel-Brunet, 86022 Poitiers cedex, France
[b] Platform for Research and Analysis in Environmental Sciences, Doctoral School of Science and Technology, Faculty of Sciences, Lebanese university, P.O. Box 5, Campus Rafic Hariri, Hadath, Beirut, Lebanon
[c] Geobiostratdata, Consulting, 385, route du Mas-Rillier, 69140 Rillieux-la-Pape, France

ARTICLE INFO

Article history:
Received 15 June 2016
Accepted after revision 17 August 2016
Available online 4 November 2016

Handled by François Chabaux

Keywords:
Karst
Groundwater
Karst infillings
Black clays
Sedimentary organic matter

ABSTRACT

The selenium (Se) content and the associated release mechanisms in both surface and groundwater have become a major concern worldwide over the past 30 years. Within the Hydrogeological Experimental Site of Poitiers (HESP), a large range of aqueous Se concentrations (from non-detectable to more than 30 ppb) is observed in a limited area (about 10 ha), where water flows are highly characterized. This site thus consists of an interesting spot to better understand the release mechanisms of selenium into groundwater. The present study consists of an identification and a characterization of the lithological sources of Se within the HESP. Total rock analyses applied to core samples from different depths and wells demonstrated that selenium is concentrated in argillaceous sediments enriched with organic matter, pyrite and uranium that fulfill a part of the karst cavities developed within the Bajocian host rocks. Mineralogical and petrographic investigations highlighted the heterogeneity of these filling materials and showed the presence of successive deposits under different climatic conditions. Extensive characterizations dated the selected Se-rich samples from the Upper Cretaceous and converged to demonstrate the external and continental origin of the studied filling materials and their transformation after deposition under reduced conditions. Only indirect correlations allow considering an agreement between the Se history and the very mature organic matter identified in the argillaceous samples. This association will be further favored to determine the mechanisms releasing selenium into groundwater.

1. Introduction

Although average selenium concentrations in the continental crust are relatively low (0.05 ppm), diffuse geogenic pollutions are widely observed (Coleman and Delevaux, 1957; Yang et al., 1989; Presser et al., 1994; Seby

* Corresponding author. CNRS, UMR 7285, Institut de chimie des milieux et matériaux de Poitiers (IC2MP), Université de Poitiers, bâtiment B8, rue Michel-Brunet, 86022 Poitiers cedex, France.
E-mail address: joseph.bassil@univ-poitiers.fr (J. Bassil).

http://dx.doi.org/10.1016/j.crte.2016.08.004

et al., 1998). Selenium is in fact an important micronutrient with a narrow range between its toxic and deficiency concentration (Barron et al., 2009; Levander and Burk, 2006). Se intake for animals and humans is mainly provided by meats, cereals and, to a lesser extent, by drinking water (Appleton et al., 2006). Human intake is indirectly related to the selenium content in natural waters and to the bioavailable fraction of selenium in soils and geological materials that can be easily transferred to water and biota.

The geographical distribution and availability of Se in soils and natural waters is largely uneven and linked to the variable concentrations in rocks, as already recently emphasized by Schmitt et al. (2012) for other elements such as Mg, Ca, Li, and B, and for their isotopic signature. Limestone, sandstone, mafic and ultramafic rocks, intrusive and extrusive acid rocks often contain low Se concentrations (Coleman and Delevaux, 1957). In contrast, coals, shales, argillaceous sediments and phosphate rocks could be enriched with selenium (Coleman and Delevaux, 1957; Fernández-Martínez and Charlet, 2009; Vesper et al., 2008).

Selenium can thus be highly concentrated in black organic-rich shales and seleniferous black shales that are the geological parent material of the widespread seleniferous soils in the United States and in Europe (De Temmerman et al., 2014).

In natural waters, selenium concentrations are generally lower than 1 ppb (Ralston et al., 2008), but may significantly increase, influenced by anthropic or geogenic sources to reach toxic levels (Charlet et al., 2007; Fernández-Martínez and Charlet, 2009). The main aqueous selenium chemical speciation corresponds to the most labile and bioavailable forms: the oxyanions selenites (Se^{IV}) and selenates (Se^{VI}) (Ralston et al., 2008). Selenium speciation strongly depends on pH and Eh (Masscheleyn et al., 1990). Hence, selenium has a complex behavior and a large variety of selenium compounds may be found in the environment (Fernández-Martínez and Charlet, 2009; Masscheleyn et al., 1990; Ralston et al., 2008; Seby et al., 1998).

In France, the selenium concentration limit for safe drinking water has been set at 10 ppb, but in several areas this limit is exceeded (Chabart et al., 2006; Gourcy and Winckel, 2010; Karnay, 1999; Vernous et al., 1998). In the East and the West of the Paris Basin, geogenic sources of Se were identified and the enrichment of water by Se is considered as a result of oxidation processes after the drilling of wells (Gourcy and Winckel, 2010; Gourcy et al., 2011). In the French Department of Vienne, selenium anomalies (up to 40 ppb) were observed in different water distribution units and were attributed to the presence of continental selenium-rich facies formed by gravels and silty clay (Barron et al., 2009; Karnay, 1999).

This work presents a study that aims to identify and characterize the potential lithological source of selenium in the well-characterized limestone aquifer of the Hydrogeological Experimental Site of Poitiers (HESP), France.

2. Settings

The Hydrogeological Experimental Site of Poitiers (HESP) is a field research facility whose primary objective is to support the development of characterization methods and modelling approaches for groundwater flow and solute transport in heterogeneous carbonate aquifers, as a basis for the protection and management of groundwater resources. Hydrogeological and hydrogeochemical investigations focus on a confined limestone aquifer, which has been extensively characterized over an area of approximately 10 ha.

The HESP is located in a geological area called "Poitou Threshold" (Gabilly and Cariou, 2007), which makes the transition between two large Mesozoic–Cenozoic sedimentary basins, i.e. the Paris Basin to the northeast and the Aquitaine Basin to the southwest (Fig. 1). The Poitou Threshold consists of Jurassic carbonate rocks lying on a Hercynian crystalline basement. On the HESP area, the sedimentary cover begins with around 20-m-thick Aalenian dolomitic limestone and dolomite. These facies are overcome by the Bajocian limestone formations (50–60 m). Bathonian and Callovian rocks were completely eroded southward Poitiers, and the Cretaceous sedimentary formations are completely eroded in the region.

Karst cavities partially filled with dark deposits are also present, and evidences based on the directional analysis of cave maps (Bodin and Razack, 1997) support the occurrence of karstification after the Cenozoic Pyrenean and Alpine tectonic phases.

Two limestone aquifers of regional extent occur in the Jurassic carbonate series:

- the Lower- and Middle-Lias aquifer;
- the Dogger aquifer.

These two aquifers are separated by the Toarcian aquitard consisting of low-permeability marls. The thickness of the Lower- and Middle-Lias aquifer is about 25 m, whereas the Toarcian aquitard and the Dogger aquifer are around 10 and 100 m thick, respectively. Previous works have demonstrated that these two aquifers are well isolated from each other by the Toarcian marls (Bodin et al., 2012; Chatelier et al., 2011). Furthermore, the coupling between flowmeter logs, borehole imaging logs

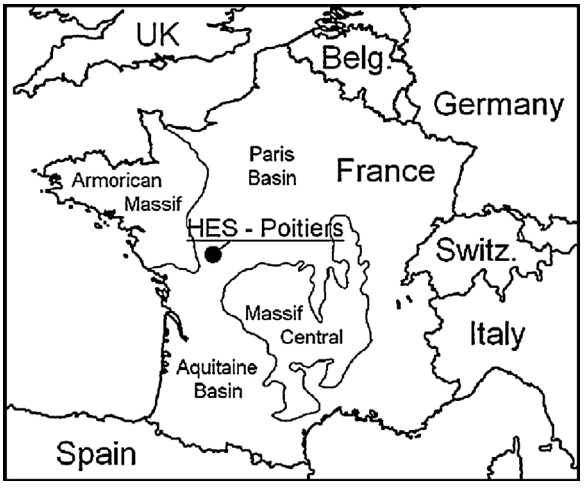

Fig. 1. Location of the HESP in France.

Table 1
Concentrations of Se, SiO_2, Al_2O_3, CaO, FeO, total sulfur, organic carbon and uranium in the samples from the C4 and the C5 wells.

Age	Sample	Depth (m)	Description	Se (ppm)	SiO_2 (%)	Al_2O_3 (%)	CaO (%)	FeO (%)	S (%)	Corg (%)	U (ppm)
Quaternary/ Tertiary	**C4 Qu1**	9.97	Conglomerate + shale + sandstone	0.18	51.61	10.01	0.70	< 0.05	< 0.01	< 0.01	6.75
	C4 Qu2	15.98	Conglomerate + shale + sandstone	0.05	66.74	12.57	0.87	< 0.05	< 0.01	< 0.01	4.39
	C4 Qu3	18.11	Conglomerate + shale + sandstone	1.72	53.77	15.16	0.52	< 0.05	< 0.01	< 0.01	6.83
Bathonian	**C4 Bt1**	20.49	Limestone	0.07	0.40	0.07	55.84	< 0.05	0.03	0.03	2.78
	C4 Bt2	26.24	Silicified limestone	0.28	2.23	0.20	54.73	0.07	0.02	0.03	1.46
	C4 Bt3	31.56	Silicified limestone	0.03	1.19	0.30	55.25	0.07	0.01	0.02	3.79
	C4 Bt4	35.67	Silicified limestone	0.05	0.78	0.13	55.91	0.05	0.03	0.04	1.72
	C4 Bt5	40.57	Silicified limestone	0.21	0.71	0.09	56.00	< 0.05	0.02	0.04	2.33
	C4 Bt6	46.51	Limestone	0.07	0.17	0.15	56.10	< 0.05	0.03	0.05	1.40
Bajocian	**C4 Bj1**	50.88	Limestone	0.11	0.06	0.08	56.25	0.03	0.03	0.04	1.55
	C4 Bj2	55.76	Limestone	**28.00**	0.07	0.13	55.61	0.14	0.07	0.06	3.11
	C4 Bj3	57.81	Argillaceous/Marly limestone	**153.00**	59.99	16.09	6.42	0.53	0.34	**0.91**	27.28
	C4 Bj4	61.68	Limestone	0.19	0.58	0.35	54.71	0.10	0.02	0.03	1.54
	C4 Bj5	67.71	Limestone	0.14	0.59	0.34	54.85	0.11	0.23	0.07	7.07
	C5 Bj1	**67.86**	Argillaceous	**1.70**	15.57	12.00	34.18	0.8	3.02	**2.94**	406.28
	C5 Bj2	**69.36**	Argillaceous	**2.10**	39.49	29.23	1.22	1.5	5.98	**7.51**	912.60
	C4 Bj6	72.14	Argillaceous/Marly limestone	**6.40**	1.38	0.65	53.96	0.09	0.04	0.06	0.53
	C4 Bj7	74.88	Argillaceous/Marly limestone	**8.10**	33.02	24.23	14.44	0.46	0.13	**0.57**	25.94
	C4 Bj8	82.23	Argillaceous/Marly limestone	**10.50**	0.83	0.42	54.70	0.10	0.04	0.04	0.58
	C4 Bj9	86.04	Limestone	0.11	2.41	0.63	52.58	0.20	0.36	0.09	24.73
	C4 Bj10	91.50	Argillaceous/Marly limestone	**6.10**	25.10	9.37	15.90	1.86	13.17	**0.73**	12.58
	C4 Bj12	92.58	Limestone	**3.80**	13.85	7.81	32.02	1.42	3.72	**1.08**	18.53
	C4 Bj13	93.29	Argillaceous	**495.00**	34.26	21.86	4.17	2.52	7.26	**1.22**	36.09
	C4 Bj14	94.81	Argillaceous	0.05	0.83	0.48	54.37	0.15	0.02	0.04	1.16
	C4 Bj15	96.38	Limestone	0.14	4.12	1.07	51.56	0.20	0.03	0.04	2.96
	C4 Bj16	102.13	Argillaceous/Marly limestone	0.12	1.91	0.54	35.89	0.61	0.36	0.10	3.25
Aalenian	**C4 Aa1**	105.50	Limestone	0.04	2.35	0.55	52.45	0.22	0.17	0.07	2.82
	C4 Aa2	110.72	Limestone	0.17	2.86	0.60	43.59	0.42	0.65	0.12	3.00
	C4 Aa3	115.67	Limestone	0.09	6.96	1.02	30.45	0.54	0.53	0.13	1.40
	C4 Aa4	119.02	Cherty limestone	0.12	12.64	2.38	40.54	0.31	1.11	0.27	2.53

and fluid temperature/conductivity logs indicates that the groundwater flow in the Dogger aquifer is strongly constrained within a three-dimensionally interconnected network and the low storativity values indicate that the Dogger aquifer is currently locally confined.

Water sampling campaigns between 2007 and 2012 revealed significant differences of aqueous total selenium content between wells located only a few tens meters from each other, from amounts lower to 5 ppb (detection limit) to more than 25 ppb. The HESP thus consists of an interesting area for the understanding of the Se behavior into a well-characterized aquifer.

3. Materials and methods

3.1. Rock sampling

A first set of samples was extracted from the C_4 borehole drilled in 2004 (Table 1). These samples being stored at ambient room conditions, a partial alteration of these samples – mainly of the originally organic matter – has presumably occurred, limiting the investigations on the C_4 samples to mineralogical and geochemical studies. The samples from Quaternary and Tertiary ages present specific anomalies (available as Supplementary Material, see Figs. 1 and 2, and Table 1) that will not be discussed in the present paper.

During the drilling of the C_5 well (2012), fresh samples were collected as cylinders of 10 cm diameter per 15 cm length and stored under anaerobic atmosphere (argon) at low temperature (–18 °C). Extensive studies were performed on two C5 argillaceous samples from different depths.

3.2. Mineralogy

Powders were obtained by grinding in an agate mortar to get the infra 50 μm fraction, while oriented preparations were obtained from suspensions in osmosed water under ultrasonic treatment. The mineralogical study of the samples was performed following the standard powder

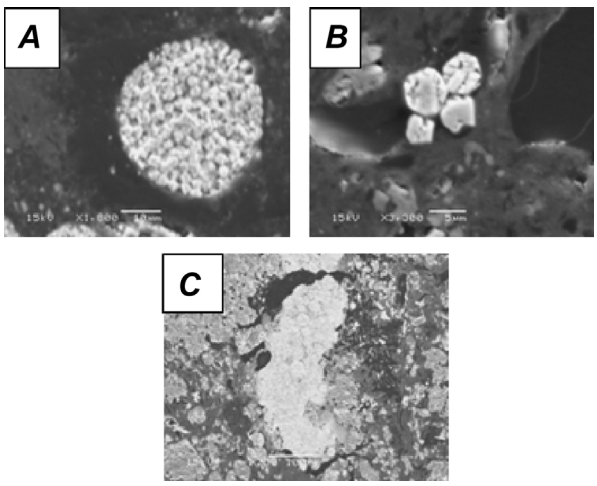

Fig. 2. Main identified pyrite morphologies (secondary electron images). *A. Framboïdal pyrite. B. Euhedral pyrite. C. Elongated pyrite.*

procedures outlined by Brindley and Brown (1980) and Moore and Reynolds (1997) for X-ray diffraction (XRD) analysis. The oriented preparation are analyzed after being air dried and after vapor salvation with ethylene glycol at 60 °C for 12 hours and heat for 4 hours at 350 °C and 550 °C. The diffractogram patterns were acquired with a Philips Panalytical X'pert Pro apparatus using copper Cu Kα radiation ($\lambda_{Cu\ K\alpha}$ = 1.5418 μm), a Soller slit of 0,4 rad, an antiscattered slit of 1/4°2θ, an Ni filter and an Xccelerator detector. The analytical conditions were: 40 kV, 40 mA, steps of 0,017° 2θ and 0.033° 2θ and investigated angular ranges from 2 to 65° 2θ and from 2 to 35° 2θ for powders and oriented preparations, respectively. Phase identification was made with X'pert HighScore software using JCPDS Pdf2 mineralogical database. The semi-quantifications were realized after deconvolution and integration of the main peak area of each phase using Fytyk software.

3.3. Elemental analysis

Elemental analysis was performed on powered samples representing all the geological facies of the C_4 well and the two fresh clayey powdered samples (C5Bj1 and C5Bj2) of the C_5 well. The samples were analyzed at the SARM laboratory (CRPG, CNRS, Nancy, France). Elemental compositions were obtained after $LiBO_2$ fusion and acid dissolution. Major elements were quantified by ICP–AES Thermo Fischer Cap 6500 and trace elements by ICP-MS Agilent 7700XI, following the methods described by Carignan et al. (2001). Total organic carbon (after treatment with concentrated HCl to remove inorganic carbon) and total sulfur were determined using a carbon–sulfur elemental analyzer LECO SC 144DR (CRPG, CNRS, Nancy, France).

The number of data (inferior or equal to 30 per element) is insufficient to realize a multivariable analysis and statistical studies were only realized using Pearson correlations coefficients calculated using "$R^{3.0.2}$" software between the normalized values of the elemental contents.

3.4. Petrography

To prepare standard-type thin sections (26 mm × 46 mm), the frozen samples were cut off by dry sawing before impregnation at room temperature under atmospheric pressure with a two-component glue composed of a polymerizing agent (Araldite) and 20% acetone. The thin sections were first observed using an optical polarized light microscope to investigate the rock structure and the different sedimentary figures. After carbon coating, the samples were then observed using a scanning electron microscope JEOL 5600-LV [Low Vacuum] (IC2MP, Poitiers) equipped with a secondary electron detector Everhart–Thornley and a backscattered electron detector Centaurus (KE Development ic, Cambridge) with a Bruker energy dispersive X-ray spectrometer for scanning electron microanalyses (SEMA). Data processing was provided by chemical analysis software QUANTAX. The petrographic investigation focuses on the identification, location and description of significant minerals morphologies and tends to define the distribution of selenium into the matrix.

3.5. Organic matter analysis

A molecular characterization of the organic matter was performed by thermochemolysis coupled with a GC–MS on the C5 samples. The experimental method described by Grasset and Amblès (1998) was applied to powdered samples (2.5 g) placed in a ceramic boat with an excess of a 50% (w/w) methanol solution of tetramethylammonium hydroxide (TMAH). The sample was left stand for 1 h to allow the TMAH solution to fill all the pores. Then the boat was placed in a Pyrex tube and heated at 400 °C for 30 min in a tubular furnace. Thermochemolysis products were then swept by nitrogen N_2 (flow rate: 100 mL/min) to a trap containing dichloromethane. After heating, the pyrolysate was transferred quantitatively into a round-bottom flask, vacuum-dried, weighed, and re-dissolved in dichloromethane and stored at 0 °C until GC–MS analysis.

Gas Chromatography–Mass Spectrometry analysis was achieved with a Trace GCThermo Finnigan (split injector, 250 °C; FID, 300 °C) with a fused silica capillary column (Supelco Equity 5%, 30 m in length, 0.25 mm i.d., 0.25 m in film thickness), and helium as the carrier gas. The oven was initially kept at 60 °C for 1 min, and then heated at a rate of 5 °C·min^{-1} to 300 °C and maintained at that temperature for 15 min. The column was coupled with a Finnigan Trace MS quadrupole mass spectrometer (ionization energy 70 eV, mass range m/z 45–600, cycle time 1 s). The various organic products were finally identified on the basis of their GC retention times, their mass spectra (comparison with standards), and the literature data.

3.6. Palynological study

The C5 samples were analyzed by Geobiostratdata, consulting company using the following conventional treatment method of argillaceous sediments for palynological studies: acid digestion successively by HCl–HF–HCl, density gradient in $ZnCl_2$, concentration by sieving at 10 μm and holding between slide and cover-slip of 50 μL of the treatment residue diluted in glycerol. The obtained slides were examined at a magnification of ×250 using a Zeiss light microscope.

4. Results and discussion

4.1. Mineralogical investigations

According to the lithology described above (see *Settings*), the most common minerals are carbonates (Table 2). Dolomite is associated with calcite at highly variable levels within Aalenian levels and at the bottom of the Lower Bajocian. Calcite is the only carbonate found in the Bathonian and, as expected, the contents of calcite drop sharply into levels corresponding to the karst infillings and in some sandy clay levels.

Within the carbonated levels, clays are only present in low quantities (0.7–2.4%) in some samples of Bajocian and Aalenian ages. Clay quantities are variable within Bajocian argillaceous infillings (4.5–79%). In carbonated levels, illite is the most abundant clay mineral except two Bajocian fillings, where smectite and kaolinite are dominant.

Table 2
Mineralogy of the carbonated and argillaceous samples.

Well	Age	Sample	Sm (%)	C (%)	I (%)	K (%)	Arg (%)	Gy (%)	Jar (%)	An (%)	Q (%)	F (%)	P (%)	Ca (%)	Do (%)	Go (%)	Py (%)
C4	*Quaternary/ Tertiary*	*C4Qu1*	3.1	0	0	0	11.6	0	0	4.4	82.8	1.2	0	0	0	0	0
		C4Qu2	58.9	0	1	40.1	50.4	0	0	3.3	46.3	0	0	0	0	0	0
	Bathonian	*C4Bt1*	0	0	0	0	0	0	0	0	0.6	0	0	99.4	0	0	0
		C4Bt2	0	0	0	0	0	0	0	0	84	0	0	15.7	0	0.4	0
		C4Bt4	0	0	0	0	0	0	0	0	1.2	0	0	98.8	0	0	0
	Bajocian	*C4Bj1*	0	0	0	0	0	0	0	0	0	0	0	100	0	0	0
		*C4Bj3**	20.6	0	0	79.4	52.2	0	0	6	27.6	1.2	0	0	0	13	0
		C4Bj4	28.1	2	43.6	26.4	0	0	0	0	0	0	0	100	0	0	0
		C4Bj5	21.1	1.2	40.8	36.9	0	0	0	0	0	0	0	100	0	0	0
		*C4Bj7**	34	0	0.6	65.4	51.5	0	0	8	2	2	0	36.5	0	0	0
		C4Bj9	0	1.3	62.4	36.3	2.7	0	0	0	1.5	0	0	94.4	0.6	0	0.8
		*C4Bj10**	49.6	0	4.8	42.7	15.7	12.4	3.3	0	13.3	1.7	0	43.7	0	5.6	4.3
		C4Bj11	0	0	47.6	52.4	2.1	0	0	0	1.6	0	0	95.5	0.7	0	0.1
		*C4Bj12**	52.8	0	17.7	29.5	4.5	3.2	1.5	0	0.7	0	0	89.2	0	0	0.9
		*C4Bj13**	51.6	1.1	20.5	26.8	16.3	6.1	0.8	0	2.4	0	0	72.5	0	0	2
		C4Bj14	78	0	7.4	14.5	1.4	0	0	0	0.7	0	0	96.2	0	1.6	0.1
		C4Bj16	22.6	4.3	36.7	36.4	1.2	0	0	0	1.4	0	0.3	13.3	83.5	0	0.3
	Aalenian	*C4Aa2*	30.3	2.1	43.7	24	0.7	0.5	0	0	5.6	0.1	0.3	0	92.2	0	0.6
		C4Aa4	0	0	56.1	43.9	0.7	0	0	0	43.5	0	0	29.7	25.7	0	0.4
C5	*Bajocian*	*C5Bj1**	0	0	0	100	19.5	0	0	2.9	0	0	0	76.6	0	0	1
		*C5Bj2**	8	0	0	92	79	0	0	14.8	3.7	0	0	0	0	0	2.5

Sm: smectite; C: chlorite; I: illite; K: kaolinite; Arg: total clays (peak at 4,45–4,50 Å); Gy: gypsum; Jar: jarosite; An: anatase; Q: quartz; F: K-feldspar; P: plagioclase; Ca: calcite; Do: dolomite; Go: gœthite; Py: pyrite; *: Karst infillings.

Kaolinite is dominant in Upper and Middle Bajocian infillings, while smectite is the most abundant clay mineral in Lower Bajocian infillings.

The detrital assemblage is mainly composed of quartz. In levels where this mineral is most expressed, it is usually associated with microcline, except in the Aalenian and the Lower Bajocian bottom, where an albite-type plagioclase is present. In the Bajocian argillaceous levels, quartz may be associated primarily with anatase and small amounts of other heavy minerals, such as zircon and rutile, identified by XRD and SEM-EDX.

The Lower and Middle Bajocian terranes are further characterized by the presence of iron-rich minerals, with pyrite (FeS_2) generally associated or not with gœthite, and sulfates, mainly small amounts of gypsum accompanied by jarosite. In the Lower Bajocian, pyrite and sulfates are found both in the host limestone and in the karst infillings. Sulfates are absent in karst infillings located in limestones of the Middle to the Upper Bajocian. Finally, gœthite is only well expressed in the sandy clay level.

The differences in clay type can demonstrate that the argillaceous infillings are not originated from a simple dissolution of the limestone, because the weathering of a parental rock does not produce the same original argillaceous assemblages (Velde and Meunier, 2008). The high quartz quantities in some argillaceous levels and the presence of other detrital minerals such as anatase, zircon and rutile also support a detrital origin of these argillaceous infillings.

4.2. Occurrence of selenium in the HESP

Se-enriched zones were attributed to samples with Se content above 1 ppm. Such samples are observed in some Bajocian levels (Table 1) along with a depletion of calcium and inorganic carbon (not shown), which corresponds to the carbonated aquifer. On the contrary, these samples present a considerable enrichment in silicon and aluminum, consistent with the presence of clays as the most abundant phases of these levels. The exceptions – samples C4Bj2, C4Bj6 and C4Bj8 – correspond to the border samples between the limestone host rock and the identified selenium-enriched argillaceous levels. The argillaceous levels are therefore suspected to be the main carrier matrix of selenium in the Dogger's aquifer.

The argillaceous levels rich in selenium are consistent with the three karstified levels described by Audouin et al. (2008) at approximately 50, 80 and 110 m, suggesting that clayey matrices fulfill the main karst cavities. The argillaceous levels were identified as black clays with high values in the natural gamma log (NG > 1000 API American Petroleum Institute unit) (Keys, 1990) observed in several wells (Audouin et al., 2008). The high natural gamma logs were interpreted by the presence of high uranium content in these clays that reach 200 ppm, as calculated by the conversion of the API levels to ppm. Elemental quantifications (Table 1) show an important enrichment with uranium, but also an important heterogeneity of uranium concentrations in the argillaceous levels.

Some Se-rich argillaceous levels are also enriched with many other elements including Fe (II), sulfur and/or organic carbon. As the association of selenium with organic matter and pyrite was described by many authors (Kulp and Pratt, 2004; Martens and Suarez, 1997; Matamoros-Veloza et al., 2011), the enrichment of the argillaceous levels in selenium would therefore be easily explained by the presence of pyrite and organic matter in the argillaceous matrix. But other samples are rich in selenium and not enriched in iron, sulfur or organic carbon. The correlations are therefore more complex than a "simple" pyritic and/or an organic association, and should be consolidated by a statistical study.

Table 3
Semi-matrices of correlation of the argillaceous samples and of the limestone samples.

	Al	*As*	*C inorg*	*C org*	*Ca*	*Cs*	*Cu*	*F*	*Fe II*	*Mg*	*Mn*	*P*	*Rb*	*REE*	*S*	*Se*	*Si*	*Sr*	*U*	*V*
Al	*1.00*	0.40[b]	**−0.88**[b]	**0.86**[b]	−0.59[b]	**0.98**[b]	0.33[b]	**0.75**[b]	0.46[b]	0.30[b]	−0.25[b]	0.32[b]	**1.00**[b]	0.60[b]	**0.81**[b]	−0.21[b]	**0.96**[b]	0.38[b]	0.03[b]	0.51[b]
As	−0.18[a]	*1.00*	−0.22[b]	0.48[b]	−0.52[b]	0.38[b]	0.68[b]	0.50[b]	0.57[b]	0.43[b]	−0.09[b]	0.14[b]	0.38[b]	0.32[b]	0.62[b]	−0.09[b]	0.38[b]	−0.11[b]	−0.01[b]	0.46[b]
C inorg	−0.57[a]	0.39[a]	*1.00*	**−0.77**[b]	0.28[b]	**−0.89**[b]	−0.22[b]	−0.47[b]	−0.12[b]	0.03[b]	0.31[b]	−0.32[b]	**−0.90**[b]	−0.47[b]	**−0.70**[b]	0.21[b]	**−0.87**[b]	−0.42[b]	−0.09[b]	−0.25[b]
C org	−0.16[a]	**0.77**[a]	0.19[a]	*1.00*	−0.69[b]	**0.82**[b]	0.41[b]	0.66[b]	0.57[b]	0.46[b]	−0.31[b]	0.00[b]	**0.85**[b]	0.39[b]	**0.97**[b]	−0.14[b]	**0.91**[b]	0.19[b]	0.10[b]	0.19[b]
Ca	−0.67[a]	0.25[a]	**0.96**[a]	−0.04[a]	*1.00*	−0.54[b]	−0.35[b]	**−0.87**[b]	**−0.95**[b]	**−0.95**[b]	0.11[b]	−0.10[b]	−0.55[b]	−0.37[b]	**−0.73**[b]	0.23[b]	−0.68[b]	0.11[b]	0.05[b]	−0.39[b]
Cs	0.20[a]	**0.79**[a]	−0.17[a]	**0.86**[a]	−0.37[a]	*1.00*	0.27[b]	**0.77**[b]	0.44[b]	0.25[b]	−0.21[b]	0.44[b]	**0.99**[b]	0.60[b]	**0.76**[b]	−0.21[b]	**0.93**[b]	0.38[b]	0.04[b]	0.56[b]
Cu	0.08[a]	**0.85**[a]	0.22[a]	0.36[a]	0.17[a]	0.60[a]	*1.00*	0.25[b]	0.34[b]	0.26[b]	−0.02[b]	−0.09[b]	0.28[b]	0.21[b]	0.52[b]	−0.25[b]	0.33[b]	−0.07[b]	−0.12[b]	0.13[b]
F	0.20[a]	**0.88**[a]	−0.05[a]	**0.81**[a]	−0.23	**0.98**[a]	**0.75**[a]	*1.00*	**0.84**[b]	**0.74**[b]	0.00[b]	0.49[b]	**0.74**[b]	0.57[b]	0.67[b]	−0.25[b]	**0.76**[b]	0.08[b]	−0.05[b]	**0.70**[b]
Fe II	−0.17[a]	**0.85**[a]	−0.04[a]	0.64[a]	−0.09[a]	**0.81**[a]	**0.78**[a]	**0.85**[a]	*1.00*	**0.93**[b]	0.06[b]	0.14[b]	0.43[b]	0.31[b]	0.65[b]	−0.17[b]	0.52[b]	−0.23[b]	0.04[b]	0.47[b]
Mg	0.03[a]	**0.97**[a]	0.29[a]	**0.84**[a]	0.09[a]	**0.88**[a]	**0.79**[a]	**0.94**[a]	**0.78**[a]	*1.00*	−0.05[b]	−0.01[b]	0.25[b]	0.21[b]	0.53[b]	−0.19[b]	0.42[b]	−0.25[b]	−0.11[b]	0.26[b]
Mn	−0.65[a]	0.28[a]	**0.98**[a]	0.03[a]	**1.00**[a]	−0.33[a]	0.16[a]	−0.19[a]	−0.10[a]	0.13[a]	*1.00*	0.35[b]	−0.25[b]	−0.33[b]	−0.27[b]	0.20[b]	−0.29[b]	−0.61[b]	0.23[b]	0.28[b]
P	0.27[a]	**0.83**[a]	−0.17[a]	0.67[a]	−0.31[a]	**0.94**[a]	**0.81**[a]	**0.98**[a]	**0.88**[a]	**0.88**[a]	−0.29[a]	*1.00*	0.36[b]	0.40[b]	0.01[b]	0.04[b]	0.25[b]	−0.12[b]	0.07[b]	0.63[b]
Rb	0.02[a]	0.68[a]	−0.15[a]	**0.94**[a]	−0.35[a]	**0.94**[a]	0.34[a]	**0.86**[a]	**0.71**[a]	**0.77**[a]	−0.30[a]	**0.77**[a]	*1.00*	0.59[b]	**0.79**[b]	−0.21[b]	**0.96**[b]	0.39[b]	0.07[b]	0.52[b]
REE	**0.82**[a]	−0.42[a]	−0.36[a]	−0.65[a]	−0.32[a]	−0.30[a]	0.03[a]	−0.23[a]	−0.43[a]	−0.32[a]	−0.34[a]	−0.11[a]	−0.54[a]	*1.00*	0.39[b]	−0.29[b]	0.49[b]	0.42[b]	0.19[b]	0.53[b]
S	−0.45[a]	0.42[a]	−0.13[a]	0.12[a]	0.02[a]	0.30[a]	0.51[a]	0.33[a]	**0.78**[a]	0.24[a]	−0.05[a]	0.44[a]	0.23[a]	−0.39[a]	*1.00*	−0.21[b]	**0.86**[b]	0.09[b]	0.17[b]	0.24[b]
Se	0.48[a]	0.50[a]	−0.49[a]	**0.70**[a]	−0.68[a]	**0.92**[a]	0.36[a]	**0.84**[a]	0.60[a]	0.66[a]	−0.64[a]	**0.83**[a]	**0.87**[a]	−0.07[a]	0.10[a]	*1.00*	−0.23[b]	−0.49[b]	−0.10[b]	−0.29[b]
Si	0.44[a]	−0.64[a]	**−0.73**[a]	−0.08[a]	**−0.77**[a]	−0.05[a]	**−0.73**[a]	−0.24[a]	−0.43[a]	−0.46[a]	**−0.75**[a]	−0.25[a]	0.12[a]	0.17[a]	−0.44[a]	0.31[a]	*1.00*	0.27[b]	0.01[b]	0.37[b]
Sr	−0.54[a]	0.41[a]	**1.00**[a]	0.14[a]	**0.96**[a]	−0.18[a]	0.29[a]	−0.04[a]	−0.02[a]	0.29[a]	**0.98**[a]	−0.15[a]	−0.19[a]	−0.30[a]	−0.09[a]	−0.50[a]	−0.78[a]	*1.00*	−0.21[b]	0.16[b]
U	**0.79**[a]	0.19[a]	−0.44[a]	0.45[a]	−0.67[a]	0.64[a]	0.12[a]	0.57[a]	0.11[a]	0.43[a]	−0.60[a]	0.54[a]	0.57[a]	0.31[a]	−0.43[a]	**0.84**[a]	0.49[a]	−0.45[a]	*1.00*	0.15[b]
V	0.62[a]	0.57[a]	-0.40[a]	0.59[a]	-0.59[a]	**0.89**[a]	0.56[a]	**0.88**[a]	0.60[a]	**0.72**[a]	-0.55[a]	**0.89**[a]	**0.74**[a]	0.15[a]	0.07[a]	**0.95**[a]	0.12[a]	-0.38[a]	**0.85**[a]	*1.00*

Significant correlations (positive and negative) are highlighted by a bold font.
[a] Argillaceous samples.
[b] Limestone samples.

4.3. Correlation analysis and selenium distribution

The present correlation analysis (Table 3) is consistent, for major elements such as Ca, Si or Al, with the lithological description and the mineralogical studies (Table 2). For instance, within the "limestone" samples, negative correlations between Ca and Mg (–0.95) or reduced iron Fe^{II} (–0.95) are coherent with the presence of dolomite and ferrous carbonates that substituted calcium carbonate in the Aalenian levels and at the bottom of the Lower Bathonian.

Within the limestone aquifer, no element is significantly correlated with selenium, probably disseminated between different structural components (Table 3, top). However, selenium concentrations are relatively low (Table 1) in the limestone host rock samples, and high positive anomalies are only observed in the "argillaceous" and "border" samples.

Literature data generally reported selenium affinities for pyritic materials, and more generally for metallic sulfide minerals (Fernández-Martínez and Charlet, 2009; Perkins and Foster, 2004; Wang et al., 2010), but also for mature organic matrices like coals (Coleman et al., 1993; Finkelman et al., 1999) and for phosphates (Fernández-Martínez and Charlet, 2009). When focusing on "argillaceous" levels (Table 3, bottom), selenium is well correlated with P (0.83), moderately with C_{org} (0.70) and Fe^{II} (0.60), which could be consistent with a distribution between the pyritic, apatite and organic materials present in the matrix. Selenium is also well correlated with U (0.84) and surprisingly highly correlated with vanadium (0.95), alkali metals (Cs [0.92] and Rb [0.87]) and fluorine (0.84). If a chemical affinity is highly unlikely, the abundance of selenium and of these elements is clearly concomitant. In parallel, it is interesting to note that similar high correlations are observed between these elements and organic carbon (Corg–Rb: 0.94; Corg–Cs: 0.86; Corg–F: 0.81; Corg–V: 0.59) within the argillaceous levels. Association between V and organic matter was reported for coals (Huggins and Huffman, 2004) and soils (Połedniok and Buhl, 2003). Rb and Cs have similar chemical properties and are besides strongly correlated (0.94). The association between Cs and organic matter has already been described in soils (Mabit and Bernard, 1998; Takenaka et al., 1998; Tegen and Dörr, 1996) and organic groundwater colloids (Caron et al., 2008). The affinity of these two alkaline elements with organic matter may indirectly explain their affinity for selenium, through the presence of ternary complexes for instance (Gustafsson and Johnsson, 1994).

Other elements present high correlations with the organic carbon and could be used to better define the nature of organic matter. Within the "limestone" aquifer, organic carbon is well correlated with Si (0.91) and Al (0.86), and especially with sulfur (0.97), which presumably corresponds to a marine-influenced diagenesis environment, where high concentrations of sulfate and iron salts in marine water leads to the formation of pyrite and organic sulfur (Wang et al., 2008; Wang et al., 2010). These correlations are not observed in the "argillaceous" filling materials (Corg–Si:–0.08; Corg–Al:–0.16; Corg–S: 0.12).

As for the organic C, most of the correlations within the "limestone" aquifer are distinguishable from the "argillaceous" samples, which demonstrates that the filling materials have an external origin and are not simply originated from the dissolution of the host rock. This tendency is particularly observed for iron, which is weakly correlated with S (0.65), As (0.57) and Cu (0.34), and strongly correlated with Mg (0.93), due to its carbonated nature in the "limestone" samples, whereas high correlations with S (0.78), Cu (0.78) and As (0.85) are observed in the "argillaceous" levels, probably due to an incorporation of these elements in pyrite during its early stage of formation (Huerta-Diaz and Morse, 1992; Morse and Arakaki, 1993) or to their presence as sulfide microinclusions (Deditius et al., 2010; Large et al., 2009).

The correlation analysis thus confirmed that the argillaceous infillings are detrital sediments from terrestrial external origin: they are not originated from the limestone local rocks alteration. Within the argillaceous sediments, selenium should be mainly associated with the organic fraction.

4.4. Extensive characterization of the karst infillings

4.4.1. Petrographic investigations

The black clayey samples present an alternation of inhomogeneous depositions observed as non-parallel crossed laminations more or less rich in carbonates or clays. Carbonate minerals are present from submillimetric to millimetric grains either as fossil fragments or as grains (< 0.1 mm) that probably belong to the matrix background. A part of the carbonates would thus have precipitated in situ.

Clays appear as homogeneous millimetric light areas separated by dark brown millimetric laminations. Elemental analysis shows a chemical composition similar to those of pure kaolinite in homogeneous domains and mixtures of kaolinite and smectite minerals, but also quartz, iron oxides, and calcite in dark zones. Within the laminated argillaceous deposits, organic matter appears as black or dark brown patches.

Three main morphologies of pyrite (Fig. 2) are observed, suggesting different ways of their formation (Raiswell, 1982). Framboidal pyrite, isolated or in clusters, is the main type encountered. These crystals have a composition similar to the theoretical formula of pyrite (FeS_2), without detectable substitution of sulfur by selenium. The formation of framboidal pyrite is interpreted as a combination of biotic and inorganic processes (Wilkin, 1995). Large framboidal pyrite – from 4 to 50 μm – is generally formed in pore water of anoxic sediments during diagenesis, while smaller framboidal pyrite (< 6 μm) is formed in anoxic water and then buried in the sediments (Wilkin and Barnes, 1997). As most of the pyritic crystals observed in the samples from the C5 well have large diameters, a formation in the porosity after deposition is assumed. These crystals were then probably preserved after an early diagenetic stage and a rock-forming process (Pierret et al., 2000; Wilkin et al., 1996).

Less commonly observed are euhedral pyrite crystals that could be directly formed by nucleation and growth in

supersaturated solution (Giblin and Howarth, 1984) or are transformed from FeS precursor precipitated from an initial supersaturated solution (Schoonen and Barnes, 1991). Elongated framboidal pyrites were only identified in relatively carbonated-rich levels and consist of spherical pyrite crystals cemented with uranium phosphate abundantly present in the spaces between the spheres. The association between pyrite and uranium was observed in uranium ores (Cunningham et al., 1998; England et al., 2001; Simpson and Bowles, 1977). No uranium ore was described in the Poitou threshold, suggesting a transportation of these materials probably from the Massif Central or the Armorican Massif (Fig. 1).

Abundance of titanium oxides, zircons, and quartz emphasizes the detrital origin of these deposits. Most rarely, calcium phosphates were identified; their presence may be of biological origin or result from igneous rocks erosion. Organic matter was also observed disseminated between the carbonated and the argillaceous areas or as dark brown filling cavities of homogenous color, suggesting a dissociation of organic and mineral matters in some areas.

Organic matter areas, argillaceous zones rich in organic matter, apatite and pyrite are all potential candidates for selenium-bearing species. Elemental mapping of these specific hosts in the studied samples was thus performed to better understand the distribution of selenium. The concentration of selenium in the samples being lower than the limit of detection of the X-ray spectrometer used in the present study, only localized positive anomalies are expected to be observable (Se concentrations higher than 0.1%). The observations of the thin sections tend to show no areas with high concentration of selenium, suggesting no specific association with a particular component of the geological matrix, but rather a diffuse distribution of selenium within the individual components.

4.4.2. Characterization of the "argillaceous" organic matter

All the analyzed argillaceous samples from the C5 well present similar chromatographic responses after thermochemolysis. The chromatogram of the thermochemolysis products derived from the C5Bj2 sample is depicted in Fig. 3. No *n*-alkane/*n*-alkene series were identified, phenols, alkylphenanthrenes and alkylanthracenes being the major products. The relative intensity of the chromatographic peaks (unresolved complex mixture – UCM) between 20 and 40 min. Fig. 3 suggests a high degree of condensation of the aromatic structures. Characteristic ions were used to examine the alkylnaphthalene and alkylphenanthrene isomers (Fig. 3).

The identified compounds could have a recent anthropogenic origin from industrial activities (Purcaro et al., 2013), but the dominant economic activities – mainly agriculture – in the local area around the HES are not coherent with this interpretation. Moreover, soils and sediments polluted by hydrocarbons should present a more complex and diversified mixture of organic hydrocarbons (Biache et al., 2014; Wakeham et al., 2003; Wilcke et al., 2014; Witt, 1995).

The phenolic nature of the degradation products agrees with the relatively low rank of the raw materials

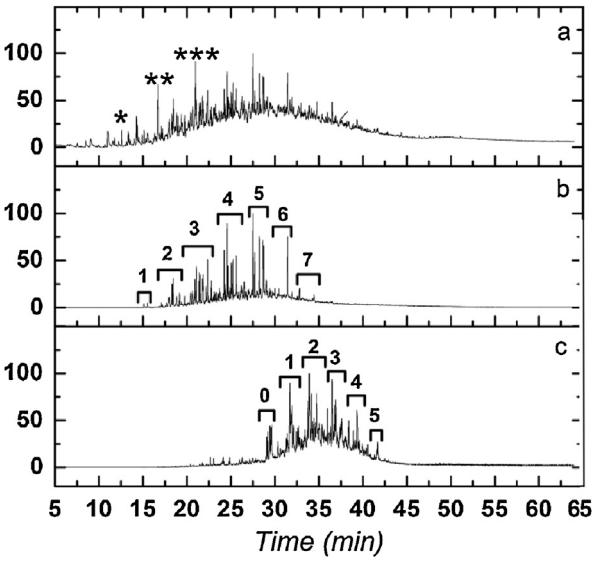

Fig. 3. Chromatogram from thermochemolysed black shales (C5Bj2). a: total Ion current Chromatogram (TIC) (*: dimethylphenol [as methoxy], **:trimethylphenol, ***: tetramethylphenol); b: extracted Ion Chromatogram (XIC) of alkylnaphtalenes ([*m*/*z*] = 142, 156, 170, 184, 198, 212 and 226]); c: extracted Ion Chromatogram (XIC) of alkykphenanthrenes ([*m*/*z*] = 192, 206, 220, 234, 248 and 262). Numbers in Fig. 3b and c indicate the number of methyl-substituted carbons.

(Hartgers et al., 1994). Phenolic compounds in the degradation products of organic sediments are usually associated with diagenetically altered lignin. It is however difficult to relate in the studied samples phenols with the structure of lignin. It should be taken into account that the organic matter present in the C5Bj2 sample cannot be unequivocally established as arising solely from woody tissues, because other sources for phenolic compounds such as tannins (Christiansen et al., 1995), which may at least in part explain the presence of the phenol isomers found here, cannot be discarded.

The distribution of phenols depends on several factors such as the initial composition of the raw organic material and the physicochemical conditions of the depositional environment. However, the maturation of the organic matter during the transformation from soft brown coal to sub-bituminous coal involves the elimination of methoxy and phenolic groups and the formation of polycyclic aromatics such as phenanthrenes and anthracenes (Philp et al., 1982), and high proportions of alkylnaphtalenes and alkylphenanthrenes were found to be dominant in mature coal (Armstroff et al., 2006).

1,2,5-Trimethylnaphtalene and 1,2,5,6-tetraramethylnaphtalene were found to be abundant in shales and coal samples (Püttmann and Villar, 1987), and 1,7-dimethylphenanthrene could derive from pimaric acid, common to plants and pine resins (Wakeham et al., 1979). In lignite coals, the presence of alkylnaphtalene was also attributed to the degradation of terpenoid and alkylnaphtalene probably derived from abiandic and sadarocopimaric acids, abundant in resins and pine forests (Fazeelat and Asif, 2005). We can thus confirm the high degree of maturation of the analyzed organic matter and affirm that

the identified phenanthrenes and naphthalenes are derived from coniferous plants.

4.4.3. Palynological investigations

Samples C5Bj1 and C5Bj2 contain enough and sufficiently well-preserved palynomorphs to be characterized. Palynological assemblages are dominated by pollens of Gymnosperms (Pinaceae, Cupressaceae, Taxodiaceae). Angiosperms are rare, thus eliminating a Neogene or Paleogene origin. Spores – mainly Pteridophytes – are abundant and frequently separated from their perispore, suggesting an input by aquatic run-off. The presence of *Cicatricosisporites* tends also to locate both samples in a Mesozoic period (Kremp and Kawasaki, 1972).

The abundance of Cupressaceae and Cyperaceae combined with the presence of *Alnus* in C5Bj1 (Leopold et al., 2012) demonstrates that the deposition of C5Bj1 is more recent than that of C5Bj2. The presence of *Classopollis* in C5Bj2 is conclusive. *Classopollis* is described from the Jurassic to the Lower Cretaceous included (Pocock and Jansonius, 1961). In the Vendée region, near to HESP site, its extinction was reported at the end of the Santonian (Azéma et al., 1981). From the Turonian to the Santonian, *Classopollis* was abundant in Vendée, and *Normapolles* was present with a high frequency. The comparison with pollen assemblages from the Vendée region allows us to date the sample C5Bj2, in which *Normapolles* is absent, from the Cenomanian, when Pinaceae pollens were abundant in Vendée (Azéma et al., 1981).

Finally, palynological assemblages suggest an Upper Cretaceous age for both samples, probably Cenomanian for C5Bj2 and Santonian to Maastrichtian for C5Bj1.

5. Conclusion: origin and history of the filling materials

This study aims to characterize the geogenic source of selenium in the HESP to further understand Se dynamics in a well-characterized Jurassic limestone aquifer. Selenium appears mainly concentrated in argillaceous sediments that fulfill some karstic cavities developed within the Bajocian host rock paleokarst.

These filling materials mainly concentrated light REE, Y, heavy elements such as Th, U and Zr, but also Se, iron, sulfur and organic carbon. A wide variability of enrichments suggests a wide variability of sources for the different elements, and thus a continental origin (Dinis et al., 2016).

Correlations between elemental analysis data allow us to distinguish many geochemical differences between "argillaceous" and "limestone" samples, which supports an external input. Markers of transport were also clearly identified in the argillaceous matrix and some of them cannot be originated from the dissolution of the limestone host rocks. The argillaceous composition proved also heterogeneous: while in the "C4 well" deep argillaceous samples are enriched in smectite, in the "C5 well" and in the "C4 well" more superficial samples, kaolinite is dominant. This indicates climate differences at the time of the formation of these minerals: kaolinite being formed in hot and moist climates, and smectite in dry climates (Eberl et al., 1984).

Organic matter is assumed to be originated from vascular plants that have been transported from the surface into karst cavities. Palynological assemblages date the C5 samples from the Upper Cretaceous, which means before the Cenozoic Pyrenean and Alpine tectonic phases, as assumed by Bodin and Razack (1997) through the directional analysis of the cave map.

Furthermore, selenium is not concentrated in a specific component of the argillaceous matrix and seems rather diffuse within the individual components. Nevertheless, reduced conditions favored after deposition the formation of pyrite crystals and the reduction of organic matter. The induced pyritic and organic materials are heterogeneous, limiting the interpretation of the correlation studies.

At last, correlative studies of total rock data demonstrated that within the argillaceous sediments, Se is highly correlated with elements (Rb, Cs, V and F) that are also correlated with organic carbon. An affinity between Se and organic matter is thus deduced. But the components extracted by thermochemolysis – GC – MS are very mature and make it difficult, at this step of the study, to deduce any chemical bonds between Se and the organic matter or the presence of organoselenide compounds. Concordances in the history of Se and the organic matter give rise to further studies to determine the nature of the Se compounds, to elucidate the nature of the affinity between selenium and the present organic matter, and to understand the mechanisms inducing the release of selenium into groundwater from this association.

Acknowledgments

The financial support of this study by the Poitou-Charentes Water Research Program (CPER #1) and by the French National Observatory System Service (NOS) H+ is gratefully acknowledged.

Appendix A. Supplementary data

Supplementary data associated with this article can be found, in the online version, at http://dx.doi.org/10.1016/j.crte.2016.08.004.

References

Armstroff, A., Wilkes, H., Schwarzbauer, J., Littke, R., Horsfield, B., 2006. Aromatic hydrocarbon biomarkers in terrestrial organic matter of Devonian to Permian age. Palaeogeogr., Palaeoclimatol., Palaeoecol. 240, 253–274.

Appleton, J.D., Zhang, Q., Green, K.A., Zhang, G., Ge, X., Liu, X., Li, J.X., 2006. Selenium in soil, grain, human hair and drinking water in relation to esophageal cancer in the Cixian area, Hebei Province, People's Republic of China. Appl. Geochem. 21 (4), 684–700.

Audouin, O., Bodin, J., Porel, G., Bourbiaux, B., 2008. Flowpath structure in a limestone aquifer: multi-borehole logging investigations at the hydrogeological experimental site of Poitiers, France. Hydrogeol. J. 16, 939–950.

Azéma, C., Fauconnier, D., Viaud, J.M., 1981. Microfossils from the Upper Cretaceous of Vendée (France). Rev. Palaeobot. Palynol. 35, 237–281.

Barron, E., Migeot, V., Rabouan, S., Potin-Gautier, M., Seby, F., Hartemann, P., Levi, Y., Legube, B., 2009. The case for re-evaluating the upper limit value for selenium in drinking water in Europe. J. Water Health 7, 630–641.

Biache, C., Mansuy-Huault, L., Faure, P., 2014. Impact of oxidation and biodegradation on the most commonly used polycyclic aromatic hydrocarbon (PAH) diagnostic ratios: Implications for the source identifications. J. Hazardous Mater. 267, 31–39.

Bodin, J., Razack, M., 1997. Application du concept de Surface Elémentaire Représentative (SER) à l'étude comparée entre karstification et tectonique dans le département de la Vienne, France. In: Jeannin, P.-Y. (Ed.), Proceedings of the 6th Conference on Limestone Hydrology and Fissured Aquifers. La Chaux-de-Fonds, Switzerland, pp. 259–262.

Bodin, J., Ackerer, P., Boisson, A., Bourbiaux, B., Bruel, D., Dreuzy, J.-R.d., Delay, F., Porel, G., Pourpak, H., 2012. Predictive modelling of hydraulic head responses to dipole flow experiments in a fractured/karstified limestone aquifer: Insights from a comparison of five modelling approaches to real-field experiments. J. Hydrology 454–455 [82–100].

Brindley, G.W., Brown, G., 1980. Crystal Structures of Clay Minerals and their X-Ray Identification. Mineralogical Society of Great Britain and Ireland, London, UK, 495 p.

Carignan, J., Hild, P., Mevelle, G., Morel, J., Yeghicheyan, D., 2001. Routine analyses of trace elements in geological samples using flow injection and low pressure on-line liquid chromatography coupled to ICP-MS: A study of geochemical reference materials BR, DR-N, UB-N, AN-G and GH. Geostand. Newsl. 25, 187–198.

Caron, S., Lucotte, M., Teisserenc, R., 2008. Mercury transfer from watersheds to aquatic environments following the erosion of agrarian soils: a molecular biomarker approach. Can. J. Soil. Sci. 88, 801–811.

Chabart, M., Gourcy, L., Braibant, G., Ghestem, J.P., Perceval, W., 2006. Origine des anomalies en sélénium dans les captages d'AEP du département de la Marne. Première approche. Rapport final, RP-54939-FR, BRGM, France, 68 p.

Charlet, L., Scheinost, A.C., Tournassat, C., Greneche, J.M., Géhin, A., Fernández-Martínez, A., Coudert, S., Tisserand, D., Brendle, J., 2007. Electron transfer at the mineral/water interface: Selenium reduction by ferrous iron sorbed on clay. Geochim. Cosmochim. Acta 71, 5731–5749.

Chatelier, M., Ruelleu, S., Bour, O., Porel, G., Delay, F., 2011. Combined fluid temperature and flow logging for the characterization of hydraulic structure in a fractured karst aquifer. J. Hydrol. 400, 377–386.

Christiansen, J.V., Feldthus, A., Carlsen, L., 1995. Flash pyrolysis of coals. Temperature-dependent product distribution. J. Anal. Appl. Pyrolysis 32, 51–63.

Coleman, R.G., Delevaux, M.H., 1957. Occurrence of selenium in sulfides from some sedimentary rocks of the western United States. Econ. Geol. 52, 499–527.

Coleman, L., Bragg, L., Finkelman, R., 1993. Distribution and mode of occurrence of selenium in US coals. Environ. Geochem. Health 15, 215–227.

Cunningham, C.G., Rasmussen, J.D., Steven, T.A., Rye, R.O., Rowley, P.D., Romberger, S.B., Selverstone, J., 1998. Hydrothermal uranium deposits containing molybdenum and fluorite in the Marysvale volcanic field, west-central Utah. Cunningham. Mineral. Deposita 33, 477–494.

De Temmerman, L., Waegeneers, N., Thiry, C., Du Laing, G., Tack, F., Ruttens, A., 2014. Selenium content of Belgian cultivated soils and its uptake by field crops and vegetables. Sci. Total Environ. 468–469 [77–82].

Deditius, A.P., Utsunomiya, S., Reich, M., Kesler, S.E., Ewing, R.C., Hough, R.M., Walshe, J.L., 2010. Trace-metal nanoparticles in pyrite. Geochim. Cosmochim. Acta 74, A216.

Dinis, P.A., Dinis, J.L., Mendes, M.M., Rey, J., Pais, J., 2016. Geochemistry and mineralogy of the Lower Cretaceous of the Lusitanian Basin (western Portugal): Deciphering palaeoclimates from weathering indices and integrated vegetational data. C. R. Geoscience 348, 139–149.

Eberl, D., Farmer, V., Barrer, R., 1984. Clay Mineral Formation and Transformation in Rocks and Soils [and Discussion]. Phil. Trans. Roy. Soc. Lond., Seri. A 311, 241–257.

England, G.L., Rasmussen, B., Krapež, B., Groves, D.I., 2001. The Origin of Uraninite, Bitumen Nodules, and Carbon Seams in Witwatersrand Gold-Uranium-Pyrite Ore Deposits, Based on a Permo-Triassic Analogue. Econ. Geol. 96, 1907–1920.

Fazeelat, T., Asif, M., 2005. Organic Geochemical Study of Lignite Coal from Salt Range Pakistan. J. Chem. Soc. Pakistan 27 (2), 199–204.

Fernández-Martínez, A., Charlet, L., 2009. Selenium environmental cycling and bioavailability: a structural chemist point of view. Rev. Environ. Sci. Biotechnol. 8, 81–110.

Finkelman, R.B., Palmer, C.A., Kolker, A., Mroczkowski, S.J., 1999. Quantifying the modes of occurrence of elementals in coal, Prospects for coal science in the 21st century. In: Bao, Q.L., Liu, Z.Y. (Eds.), Proceedings of the tenth international conference of coal sciences: Prospects for coal sciences in the 21st century. Shanxi Science and Technology Press, Tayiuan, China, pp. 21–24.

Gabilly, J., Cariou, E., 2007. Guides géologiques régionaux : Poitou, Vendée, Charentes, 2nd ed. Dunod, Paris, France, 224 p.

Giblin, A.E., Howarth, R.W., 1984. Porewater evidence for a dynamic sedimentary iron cycle in salt marshes. Limnol. Oceanogr. 29, 47–63.

Gourcy, L., Lions, J., Wyns, R., Dictor, M.C., Brenot, A., Crouzet, C., Ghestem, J.P., 2011. Origine du sélénium et compréhension des processus dans les eaux du bassin Seine-Normandie. Rapport final, RP-57344-FR, BRGM, France, 178 p.

Gourcy, L., Winckel, L., 2010. Développement de la connaissance sur le sélénium dans les nappes utilisées pour l'alimentation en eau potable en Essonne. Rapport d'avancement, RP-58589-FR, BRGM, 38 p.

Grasset, L., Amblès, A., 1998. Structural study of soil humic acids and humin using a new preparative thermochemolysis technique. J. Anal. Appl. Pyrolysis 47, 1–12.

Gustafsson, J.P., Johnsson, L., 1994. The association between selenium and humic substances in forested ecosystems – laboratory evidence. Appl. Organomet. Chem. 8, 141–147.

Hartgers, W.A., Sinnighe Damste, J.S., de Leeuw, J.W., Ling, Y., Dyrkacz, G.R., 1994. Molecular Characterization of Flash Pyrolyzates of Two Carboniferous Coals and Their Constituting Maceral Fractions. Energy Fuels 8, 1055–1067.

Huerta-Diaz, M.A., Morse, J.W., 1992. Pyritization of trace metals in anoxic marine sediments. Geochim. Cosmochim. Acta 56, 2681–2702.

Huggins, F.E., Huffman, G.P., 2004. How do lithophile elements occur in organic association in bituminous coals? Int. J. Coal Geol. 58, 193–204.

Karnay, G., 1999. Délimitation des aquifères susceptibles de renfermer du sélénium en Poitou-Charentes. Rapport, R40460, BRGM, France, 25 p.

Keys W.S., 1990. Borehole geophysics applied to ground-water investigations. US Geological Survey, Techniques of Water Resources Investigations, 2, E2, VA, USA, 149 p.

Kremp, G.O.W., Kawasaki, T., 1972. The spores of the Pteridophytes. Hirokawa Publishing Company, Tokyo, Japan, 398 p.

Kulp, T.R., Pratt, L.M., 2004. Speciation and weathering of selenium in Upper Cretaceous chalk and shale from South Dakota and Wyoming, USA. Geochim. Cosmochim. Acta 68, 3687–3701.

Large, R.R., Danyushevsky, L., Hollit, C., Maslennikov, V., Meffre, S., Gilbert, S., Bull, S., Scott, R., Emsbo, P., Thomas, H., Singh, B., Foster, J., 2009. Gold and Trace Element Zonation in Pyrite Using a Laser Imaging Technique: Implications for the Timing of Gold in Orogenic and Carlin-Style Sediment-Hosted Deposits. Econ. Geol. 104, 635–668.

Leopold, E.B., Birkebak, J., Reinink-Smith, L., Jayachandar, A.P., Narváez, P., Zaborac-Reed, S., 2012. Pollen morphology of the three subgenera of Alnus. Palynology 36 (1), 131–151.

Levander, O.A., Burk, R.F., 2006. Update of human dietary standards for selenium. In: Hatfield, D.L., Berry, M.J., Gladyshev, V.N. (Eds.), Selenium Its Molecular Biology and Role in Human Health. 2nd ed. Springer, New York, USA, pp. 399–410.

Mabit, L., Bernard, C., 1998. Relationship between soil inventories and chemical properties in a small intensively cropped watershed. C. R. Acad. Sci. Paris, Ser. IIa 327 (8), 527–532.

Martens, D.A., Suarez, D.L., 1997. Selenium speciation of marine shales, alluvial soils, and evaporation basin soils of California. J. Environ. Qual. 26, 424–432.

Masscheleyn, P.H., Delaune, R.D., Patrick, W.H., 1990. Transformations of selenium as affected by sediment oxidation-reduction potential and pH. Environ. Sci. Technol. 24, 91–96.

Matamoros-Veloza, A., Newton, R.J., Benning, L.G., 2011. What controls selenium release during shale weathering? Appl. Geochem. 26 (Suppl.), S222–S226.

Moore, D.M., Reynolds, R.C., 1997. X-Ray Diffraction and the Identification and Analysis of Clay Minerals, 2nd ed. Oxford University Press, New York, USA, 378 p.

Morse, J.W., Arakaki, T., 1993. Adsorption and coprecipitation of divalent metals with mackinawite (FeS). Geochim. Cosmochim. Acta 57, 3635–3640.

Perkins, R.B., Foster, A.L., 2004. Mineral affinities and distribution of selenium and other trace elements in black shale and phosphorite of the Phosphoria Formation. In: Hein, H.R. (Ed.), Handbook of Exploration Geochemistry, 8, Elsevier B.V, Amsterdam, The Netherlands, pp. 251–295.

Philp, R.P., Russel, N.J., Gilbert, T.D., Friedrich, J.M., 1982. Characterization of victorian soft brown coal wood by microscopic techniques and Curie-Point pyrolysis combined with gas chromatography-mass spectrometry. J. Anal. Appl. Pyrolysis 4, 143–161.

Pierret, M.C., Blanc, G., Clauer, N., 2000. On the origin of framboidal pyrite in sediments of the Suakin Deep (Red Sea). C. R. Acad. Sci. Paris Ser. IIa 330, 31–38.

Połedniok, J., Buhl, F., 2003. Speciation of vanadium in soil. Talanta 59, 1–8.
Pocock, S.J., Jansonius, J., 1961. The pollen genus Classopollis Pflug, 1953. Micropaleontology 7 (4), 439–449.
Presser, T.S., Sylvester, M.A., Low, W.H., 1994. Bioaccumulation of selenium from natural geologic sources in the Western States and its potential consequences: Environ. Manage. 18 (3), 423–436.
Purcaro, G., Moret, S., Conte, L.S., 2013. Overview on polycyclic aromatic hydrocarbons: Occurrence, legislation and innovative determination in foods. Talanta 105, 292–305.
Püttmann, W., Villar, H., 1987. Occurrence and geochemical significance of 1,2,5,6-tetramethylnaphthalene. Geochim. Cosmochim. Acta 51, 3023–3029.
Raiswell, R., 1982. Pyrite texture, isotopic composition and the availability of iron. Am. J. Sci. 282, 1244–1263.
Ralston, N.V.C., Unrine, J., Wallschläger, D., 2008. Biogeochemistry and analysis of selenium and its species. North American Metals Council, Washington, USA, 58 p.
Schmitt, A.D., Vigier, N., Lemarchand, D., Millot, R., Stille, P., Chabaux, F., 2012. Processes controlling the stable isotope compositions of Li, B Mg, and Ca in plant, soils and waters: A review. C. R. Geoscience 344, 704–722.
Schoonen, M.A.A., Barnes, H.L., 1991. Reactions forming pyrite and marcasite from solution: II. Via FeS precursors below 100 °C. Geochim. Cosmochim. Acta 55, 1505–1514.
Seby, F., Potin-Gautier, M., Giffaut, E., Donard, O.F.X., 1998. Assessing the speciation and the biogeochemical processes affecting the mobility of selenium from a geological repository of radioactive wastes to the biosphere. Analusis 26, 193–198.
Simpson, P.R., Bowles, J.F.W., 1977. Uranium Mineralization of the Witwatersrand and Dominion Reef Systems. Phil. Trans. Roy. Soc. Lond., Ser. A 286, 527–548.
Takenaka, C., Onda, Y., Hamajima, Y., 1998. Distribution of cesium-137 in Japanese forest soils: Correlation with the contents of organic carbon. Sci. Total Environ. 222, 193–199.
Tegen, I., Dörr, H., 1996. Mobilization of cesium in organic rich soils: Correlation with production of dissolved organic carbon. Water Air Soil Pollut. 88, 133–1440.
Velde, B., Meunier, A., 2008. The Origin of Clay Minerals in Soils and Weathered Rocks. Springer-Verlag, Berlin, Germany, 406 p.
Vernous, J.F., Barbier, J., Chery, L., 1998. Les anomalies du sélénium dans les captages d'Île-de France (Essone, Seine-et-Marne. Rapport, R40144, BRGM, France, 46 p.
Vesper, D.J., Roy, M., Rhoads, C.J., 2008. Selenium distribution and mode of occurrence in the Kanawha Formation, southern West Virginia, USA. Int. J. Coal Geol. 73, 237–249.
Wakeham, S.G., Forrest, J., Masiello, C.A., Gélinas, Y., Alexander, C.R., Leavitt, P.R., 2003. Hydrocarbons in Lake Washington Sediments. A 25-Year Retrospective in an Urban Lake. Environ. Sci. Technol. 38, 431–439.
Wakeham, S.G., Schaffner, C., Giger, W., Boon, J.J., De Leeuw, J.W., 1979. Perylene in sediments from the Namibian Shelf. Geochim. Cosmochim. Acta 43, 1141–1144.
Wang, J., Yamada, O., Nakazato, T., Zhang, Z.-G., Suzuki, Y., Sakanishi, K., 2008. Statistical analysis of the concentrations of trace elements in a wide diversity of coals and its implications for understanding elemental modes of occurrence. Fuel 87, 2211–2222.
Wang, L., Ju, Y., Liu, G., Chou, C.-L., Zheng, L., Qi, C., 2010. Selenium in Chinese coals: distribution, occurrence, and health impact. Environ. Earth Sci. 60, 1641–1651.
Wilcke, W., Bandowe, B.A.M., Lueso, M.G., Ruppenthal, M., del Valle, H., Oelmann, Y., 2014. Polycyclic aromatic hydrocarbons (PAHs) and their polar derivatives (oxygenated PAHs, azaarenes) in soils along a climosequence in Argentina. Sci. Total Environ. 473–474 [317–325].
Wilkin, R.T., 1995. Size distribution in sediments, synthesis and formation mechanism of framboidal pyrite (Doctoral dissertation). Pennsylvania State University, PA, USA, 454 p.
Wilkin, R.T., Barnes, H.L., 1997. Formation processes of framboidal pyrite. Geochim. Cosmochim. Acta 61, 323–339.
Wilkin, R.T., Barnes, H.L., Brantley, S.L., 1996. The size distribution of framboidal pyrite in modern sediments: An indicator of redox conditions. Geochim. Cosmochim. Acta 60, 3897–3912.
Witt, G., 1995. Polycyclic aromatic hydrocarbons in water and sediment of the Baltic Sea. Mar. Pollut. Bull. 31, 237–248.
Yang, G., Yin, S., Zhou, R., Gu, L., Yan, B., Liu, Y., Liu, Y., 1989. Studies of safe maximal daily dietary selenium intake in a seleniferous area in China II. Relation between Se-intake and the manifestation of clinical signs and certain biochemical alterations in blood and urine. J. Trace Elem. Health Dis. 3, 123–130.